

NUMERICAL INVESTIGATION OF X-45A TYPE UNMANNED COMBAT AIR VEHICLE

Haci SOGUKPINAR *^{ID}
Serkan CAG **^{ID}

Received: 29.03.2022; revised: 14.08.2022; accepted: 22.08.2022

Abstract: In this paper, the low-speed aerodynamic performance of unmanned combat air vehicle (UCAV) X-45 delta wing was investigated by a numerical method using computational fluid dynamic approaches (CFD). The investigation was conducted with X-45 and the formation of leading-edge vortices (LEV) and vortex breakdown was studied by a varying angle of attack with the range of 5° to 30° at the Reynolds number of 10,000 using the SST turbulence model and are compared with experimental data to validate simulation accuracy of CFD. Stall conditions happened at around 30°, averaged vorticity layer demonstrates a prolonged form that goes along by narrow recirculation zones neighboring to the wing surface. Detail about flow field, including LEV formation, vortex breakdown, interaction, and nonlinear aerodynamic characteristics of X-45 was presented and discussed.

Keywords: LEV, CFD, delta wing, X-45

X-45A Tipi İnsansız Muharebe Hava Aracının Nümerik Olarak İncelenmesi

Öz: Bu çalışmada, insansız savaş hava aracı (SIHA) X-45 delta kanadının düşük hızlı aerodinamik performansı hesaplamalı akışkanlar dinamiği yaklaşımları (HAD) kullanılarak sayısal bir yöntemle incelenmiştir. İnceleme X-45 ile yürütülmüş ve öncü girdapların (LEV) oluşumu ve girdap kırılması, SST türbülans modeli kullanılarak Reynolds sayısı 10.000'de 5° ila 30° aralığında değişen bir hücum açısı ile incelenmiştir. CFD'nin simülasyon etkinliğini doğrulamak için daha önceden yapılan deneysel verilerle karşılaştırılmıştır. Stol koşulları yaklaşık 30°'de meydana gelmiş, ortalama girdap katmanı, kanat yüzeyine komşu dar döngüsel bölgeleri boyunca uzanan uzun bir form göstermektedir. LEV oluşumu, girdap bozulması ve etkileşimi ve X-45'in doğrusal olmayan aerodinamik özellikleri dahil olmak üzere akış alanı hakkında ayrıntılar sunulmuş ve tartışılmıştır.

Anahtar Kelimeler: LEV, CFD, delta kanat, X-45

* Department of Electric and Energy, Vocational School, University of Adiyaman, Adiyaman 02040, Turkey

** Department of Machinery and Metal Technology Vocational School, University of Adiyaman, Adiyaman 02040, Turkey

Correspondence Author: Haci Sogukpinar (hsogukpinar@adiyaman.edu.tr)

1. INTRODUCTION

The armed and unarmed versions of unmanned aerial vehicles have gained very important progress in the last 30 years. Both versions have demonstrated their abilities as reconnaissance, used as even tactical purpose, and have been becoming an essential tool for the military operation. The Turkish-made UAV TB2 was used actively in Azerbaijan, Karabakh, and then in Ukraine, and it has been frequently mentioned by changing the war concept of the world. The delta wing structure has a relevant aerodynamic configuration that would be efficiently used at a variety of attack angles in a subsonic flow regime. Research into varied non-slender or 'low sweep' delta wing models has increased rapidly. Delta wing generates leading-edge vortices (LEV) which cause nonuniform flow field and lift distribution along the wing surface. As the increasing angle of attack, vortex breakdown happens and these decrease lift force and eventually cause flow separation and stall. These are undesirable facts for the delta wing and affect the life span of the air vehicle and must be controlled to increase aerodynamic performance. Lambourne and Bryer (Lambourne et al. 1961) observed two forms of vortex breakdown over delta wing surface as spiral and bubble but it was (Sarpkaya 1971; Faler et al. 1978) searched out three unique types of vortex breakdown: double helix, spiral, and axisymmetric (bubble) and observed that the breakdown may shift from one form to another, e.g. from a spiral to a bubble and then return spiral. The conditions under which vortex breakdown occurs are very important to know due to buffeting causing large structural vibrations and severe fatigue damage. There are various parameters affecting the vortex formation on the delta wing, such as angle of attack, yaw angle, sweep back angle, roll angle, the thickness of the wing, leading-edge geometry, Reynolds number, and free-stream conditions (Sahin et al. 2017). At the low angle of attack, a double vortex at leading-edge, circulating over the wing apex is formed by the rolling up of the viscous flow sheet [Canpolat et al. 2012]. The vortex at boundary surface causes this LEV structure, formed by the rolling of the viscous flow layer (Yaniktepe et al. 2016). This flow separation happens mainly because of the angle of attack and the sharp leading edge (Swan et al. 2006). The benefit produced by delta wing, the researcher focused on more specialized wing design e.g X45-A and lambda than simple ones. X45-A was developed by Boeing, because enemy air defense missions had to be suppressed with unmanned combat aircraft (Swan et al. 2006). Yaniktepe et al. (2016) experimentally investigated the Flow Characteristics of the X-45 and lambda delta wing planform using dye visualization, Stereoscopic Particle Image Velocity (stereo-PIV) and aerodynamic load measurements. Leading eddies were observed at low angles of attack and formed eddy flow near the wing surface similar to delta and lambda planforms. The stall was observed at the angle of attack around 32° for X45-A but the stall is prominent at fairly lower angles of attack for simple delta wing. Effects of Reynolds number on the near-surface topology of a classical UCAV X45-A planform were investigated experimentally by Elkhoury et al. (2005) and the study showed some mechanisms associated with Reynolds number dependence. Flow Structure on non-slender simple delta wing was investigated experimentally by Canpolat et al. (2009) and Yaniktepe et al. (2004). Their investigation focuses on the formation and development of LEV, vortex breakdown, and flow separation over the delta wing. Emphasis on the cross flow surface, where vortex breakdown and stall happen and these phenomena are known to be important origins of unsteady buffet loading of the wing. Simple delta wing has been studied for decades (Menter 1994) however aerodynamic characteristics of X45A-wings are rarely found in the literature.

In this study, unsteady aerodynamic characteristics of non-slender X45-A wing planform covering LEV, vortex breakdown, vorticity, flow separation, were investigated numerically by the SST turbulence model. A numerical solution was conducted by solving the conservation equation of mass and momentum. Vortical flow developed at a low angle of attack from the wing apex and rolls up on both sides of the delta wing to form LEV. Vortex breakdown, flow separation, and the stall was observed as the angle of attack increased. The numerical study was

conducted at the angle of attack from 5° to 30°. Reynolds number was specified as 10.000 for all experiments and numerical calculation.

2. NUMERICAL METHODS

The flow field over the delta wing was simulated using commercial software COMSOL. Reynolds-Averaged Navier-Stokes (RANS) equation was applied for the conservation of momentum and continuity. Turbulence effects were modeled using the Menter Shear-Stress transport (SST) model with realizability constraints. The SST model is also called the low-Reynolds number model and this model resolves the flow field down to the wall. SST model is expressed in terms of k and ω with equations (1) and (2) (Comsol, 2021;Menter 1994; Menter et al. 2003; Sogukpinar 2019; Sogukpinar 2018; Sogukpinar 2019).

$$\rho \frac{\partial k}{\partial t} + \rho u \cdot \nabla k = P - \rho \beta_0^* k \omega + \nabla \cdot ((\mu + \sigma_k \mu_T) \nabla k) \quad (1)$$

$$\rho \frac{\partial \omega}{\partial t} + \rho u \cdot \nabla \omega = \frac{\rho \gamma}{\mu_T} P - \rho \beta \omega^2 + \nabla \cdot ((\mu + \sigma_\omega \mu_T) \nabla \omega) + 2(1 - f_{v1}) \frac{\rho \sigma_\omega \omega^2}{\omega} \nabla \omega \cdot \nabla k \quad (2)$$

Where, P is the static pressure and can be represented with the equation (3).

$$P = \min(P_k, 10\rho\beta_0^*k\omega) \quad (3)$$

Here, P_k production term and it is expressed with equation (4).

$$P_k = \mu_T \left(\nabla u : (\nabla u + (\Delta u)^T) - \frac{2}{3} (\nabla \cdot u)^2 \right) - \frac{2}{3} \rho k \nabla \cdot u \quad (4)$$

Turbulence viscosity is expressed with equation (5).

$$\mu_T = \frac{\rho a_1 k}{\max(a_1 \omega, S f_{v2})} \quad (5)$$

Where, S is the characteristic magnitude of the mean velocity gradients and is expressed with the help of equation (6)

$$S = \sqrt{2S_{ij}S_{ij}} \quad (6)$$

The interpolation functions f_{v1} and f_{v2} are represented with the equation (8) and (9)

$$f_{v1} = \tanh \left(\min \left[\max \left(\frac{\sqrt{k}}{\beta_0^* \omega l_\omega}, \frac{500\mu}{\rho \omega l_\omega^2} \right), \frac{4\rho \sigma_\omega k}{\max(\frac{2\rho \sigma_\omega \omega^2}{\omega} \nabla \omega \cdot \nabla k, 10^{-10}) l_\omega^2} \right] \right)^4 \quad (8)$$

$$f_{v2} = \tanh \left(\max \left(\frac{\sqrt{k}}{\beta_0^* \omega l_\omega}, \frac{500\mu}{\rho \omega l_\omega^2} \right) \right)^2 \quad (9)$$

Where, l_ω is the distance to the closest wall. For SST, default model constants are given by (Comsol, 2021)

$$\beta_1 = 0.075, \gamma_1 = \frac{5}{9}, \sigma_{k1} = 0.85, \sigma_{\omega1} = 0.5, \beta_2 = 0.0828, \gamma_2 = 0.44, \sigma_{k2} = 1.0, \sigma_{\omega2} =$$

0.856, $\beta_0^* = 0.09, \sigma_1 = 0.31$ For this calculation flow types were set to incompressible and the gravity effect was provided in the $-z$ -direction. The chord length of the delta wing is $C=168\text{mm}$ and the sweep angle is $\Lambda = 40^\circ$. Wind speed was set to 0.058 m/s. Reynolds number was taken as 10,000 and flow over the boundary conditions of the wing was assumed to be turbulent. In a low Reynolds number model, the equations are integrated through the boundary layer to the wall, this allows the no-slip condition to be applied to the Wing surface, therefore the delta wing was modeled as a solid wall with no-slip conditions and other boundaries was modeled as a free stream. To eliminate the domain size effect on the calculation results, the computational domain size was extended at least 10 times the chord length of the model. The upstream boundary was placed 20 mean aerodynamic chords in front of the apex, 20 mean aerodynamic chords behind the tail, and 10 mean aerodynamic chords above and below the pressure and suction side. Inlet

port was set to velocity inlet and outlet was set to open boundary with zero atmospheric pressure. Mesh distribution around the delta wing is given in Figure 1. The free triangular mesh was used on the planform and triangular mesh was created on the surface. Tetrahedral mesh type was chosen in the 3D domain and maximum element growth rate was set to 1.2 from surface to boundary, more than 5 million tetrahedral mesh element was obtained around the delta wing surface. In this study, the mesh distribution was decided by making a comparison in terms of compatibility with the experimental and numerical data made before, and the studies that were compared were specified in the references. Since different images are obtained in different mesh applications, this mesh distribution correlates the experimental and numerical image was chosen. In the lower mesh distribution, the results deviate from the experimental comparisons, and in the very high mesh distribution, insolvency occurs.

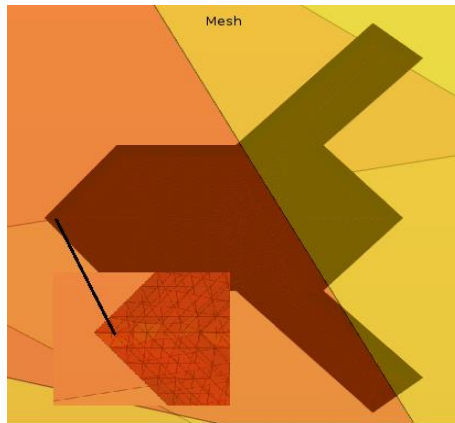


Figure 1:
Closed-up of the mesh distribution on the planform

3. RESULTS AND DISCUSSION

Figure: 2–8 shows various representations of the flow pattern on the X45-A planform at the angle of attack from 5° to 30° . The numerical results for the behavior of flow pattern in the plan-view under the different angles of attacks are given in Fig.2. Leading-edge vortices are developed at the angle of attack 5° and formed symmetrically on both side of the wing surface and closed to the side edge. Although it is seen as thin and weak at the angle of 5° the LEV becomes obvious as the increasing angle of attack. LEV up to 25° were more pronounced, fluctuations began to deteriorate LEV starting from 25° , and finally flow field was completely broken down at apex and stalled at around 30° . Flow is fairly smooth at the lower angle of attack at $\alpha=5^\circ$ and streamline continue to flow on the surface until breakdown near the aft end of the wing however when the angle of attack is increased to 10° , the flow field remained the same but the length of flow field decreased. An experiment for the X45-A with a similar configuration was conducted by Elkhoury et al. (2005) and vortex breakdown was reported at around halfway along the leading edge at the angle of 7° and vortex breakdown got closer to apex at the angle of 13° with the Reynolds number 20.000. In the current study, at $\alpha=20^\circ$ vortex breakdown is clear and the location moved forward noticeably. As the angle of attack is further increased to $\alpha = 25^\circ$, vortex breakdown was observed at around apex, and finally, by the time the angle reaches $\alpha = 30^\circ$ the burst vortex gives way to stall conditions. Fig. 3 shows side view velocity field in the middle of vortex core as a function of angle of attack. Development of LEV at the angle of attack 5° is very small, close to the surface and weak, and not identifiable, but as the angle of the attack increases, vortex radius increases and circulation widens to the rear. Plan view vorticity contour on the surface as a function of angle of attack is given in Fig. 4. At the

lower angle of attack, even if it is weak, in a small region of field where the small-scale vortex was developed at both sides of surface and also small-scale vortex formation is evident on the back left and right arm of X-45A. When the angle of attack is increased to $\alpha = 10^\circ$ the leading-edge vortex is quite pronounced and reaches from the leading edge to the middle part of the surface and the strength and area of vorticity on the arms increases. The strength of LEV increases until at the angle of 20° and the small-scale independent vortex region on the arm merged and covered each arm surface when $\alpha=20^\circ$. When the angle further increased to 25° , another vortex stronger than LEV was developed at the apex and this causes both LEVs to be merged. As the angle grows up to 30° , new vortices have formed that cover the entire surface where the LEV formation disappears.

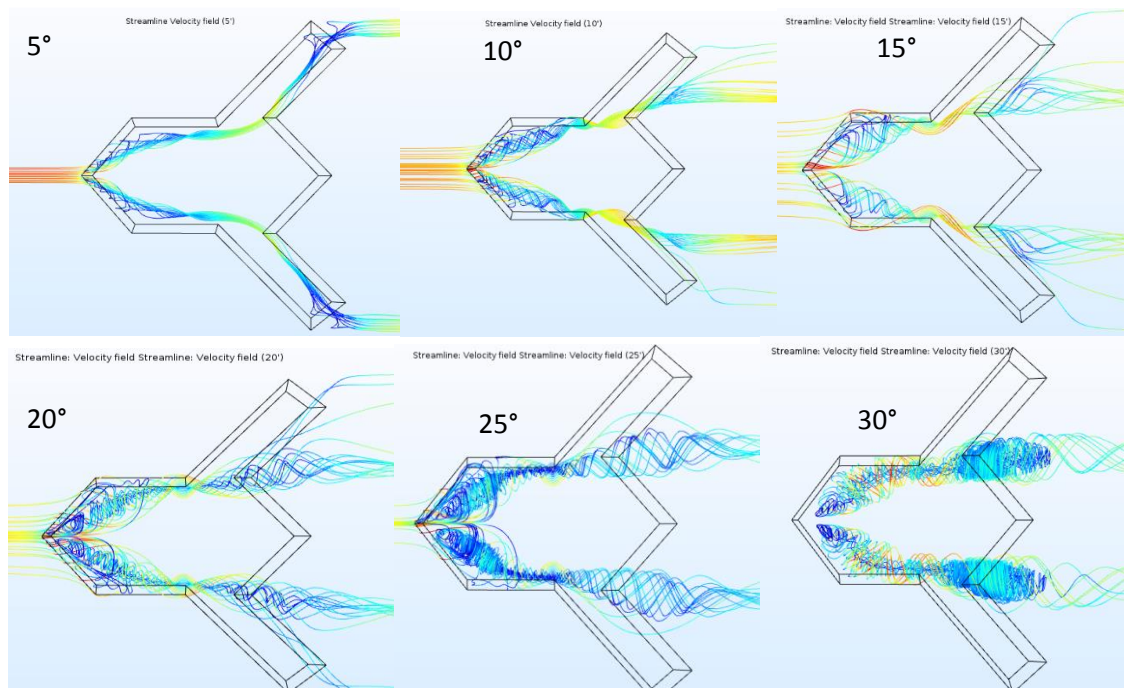


Figure.2:

Comparison of pattern of the streamline velocity field for the angle of attack from 5° to 45°

Figure:5 shows the end view pattern of the vorticity field as a function of the angle of attack from 5° to 30° on the section $x/c= 0.125$ and 0.3 respectively. Vortical flow over the wing's surface develops at the angles of attack 5° , and form close to the wing surface at $x/c=0.125$ but as the angle increases, it moves away from the surface. Swirling flow is formed on the surface starting at the angle of 15° and intensity increases with the angle. When the angle of attack increased to 30° there are several vortex areas, which are visible in the Fig. 5 ($\alpha=30^\circ$) where some are intertwined, some are formed separately and this indicates X45-A already passed to stage stall.

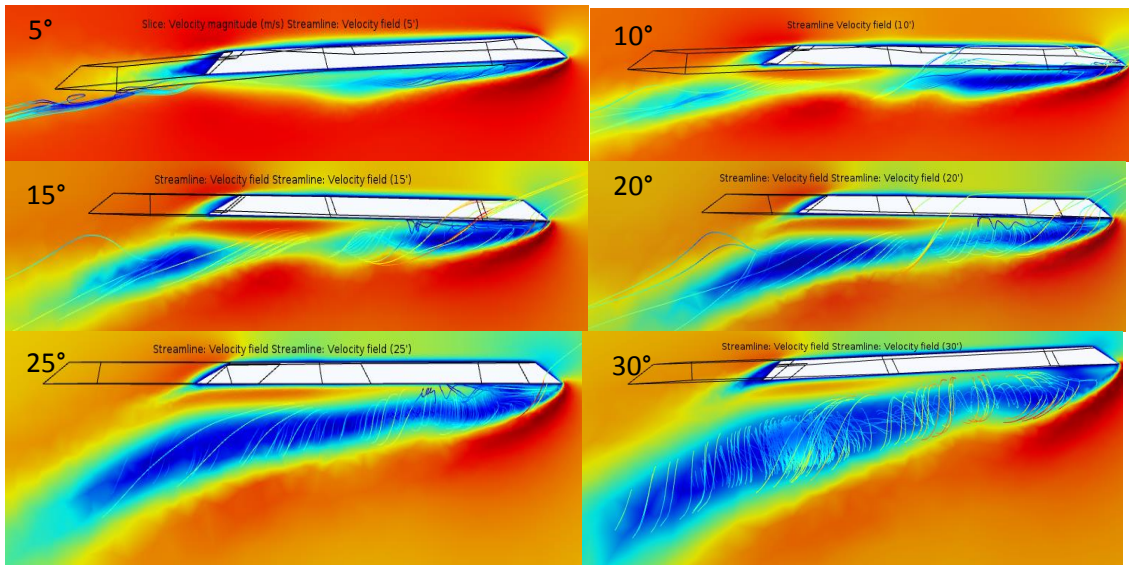


Figure 3:
Comparison of side view pattern of the velocity field in the middle of vortex core as a function of angle of attack.

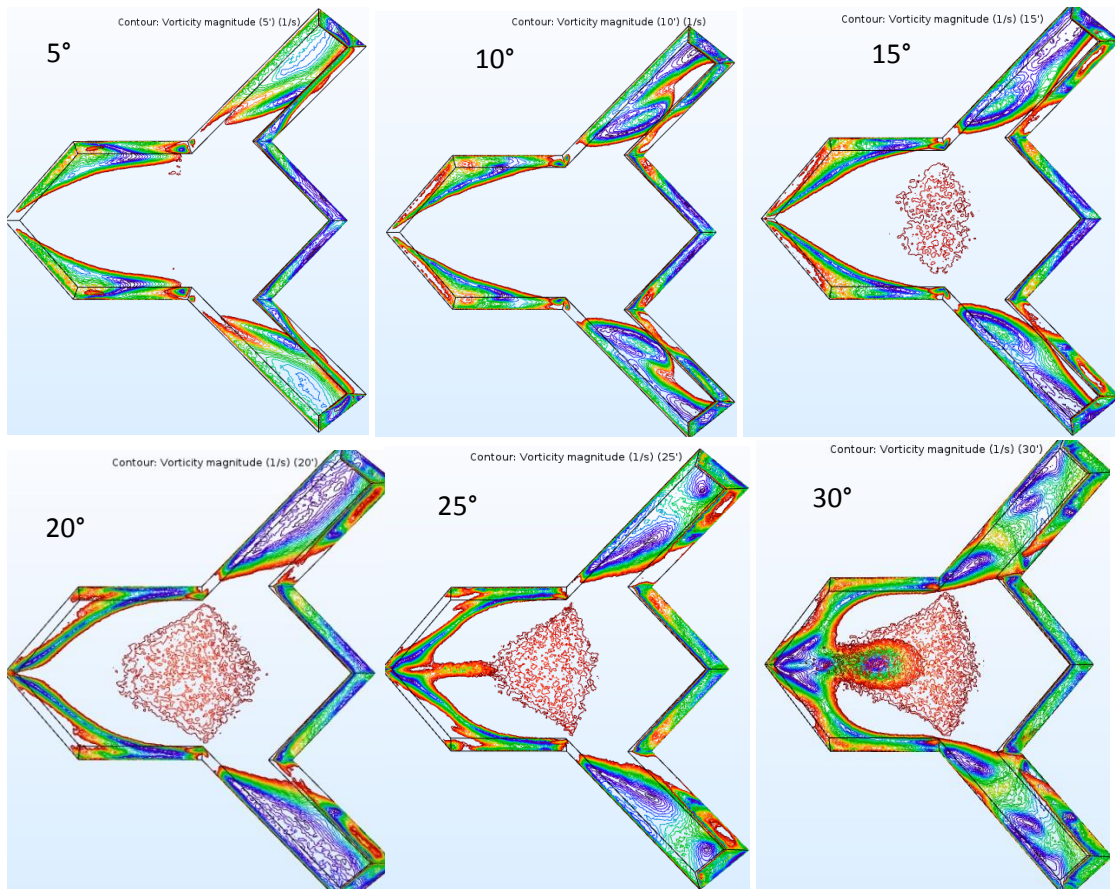


Figure 4:
Comparison of pattern of vorticity contour on the surface as a function of angle of attack.

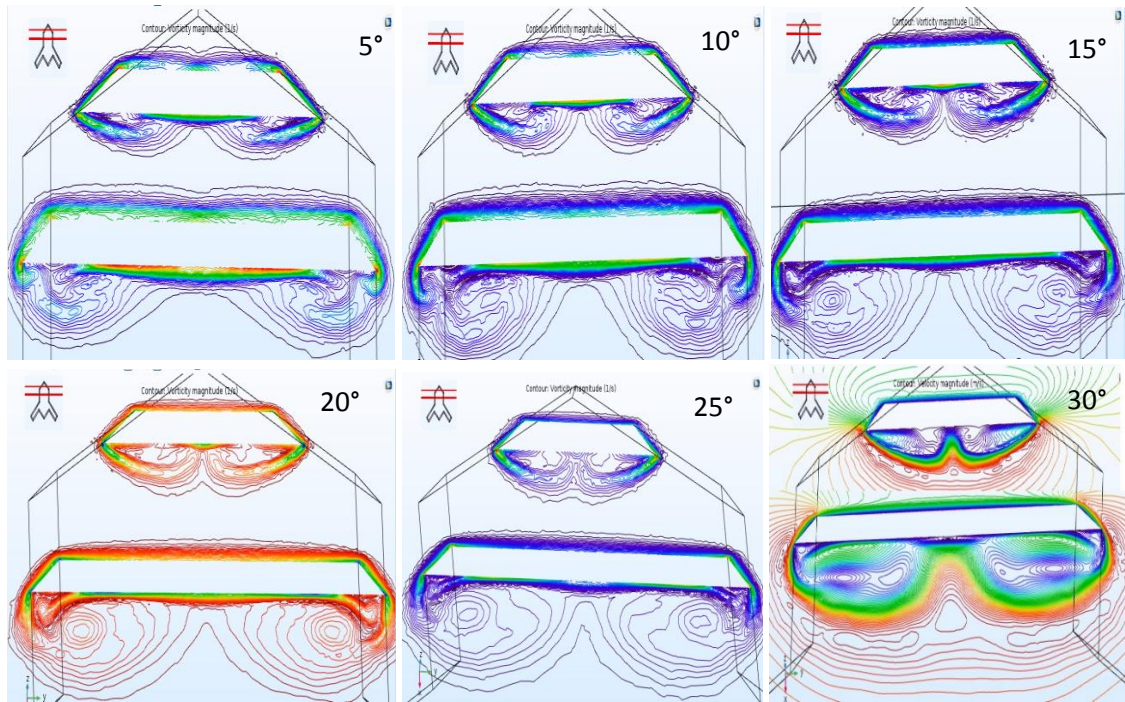


Figure 5:
Comparison of end view pattern of vorticity field as a function of angle of attack

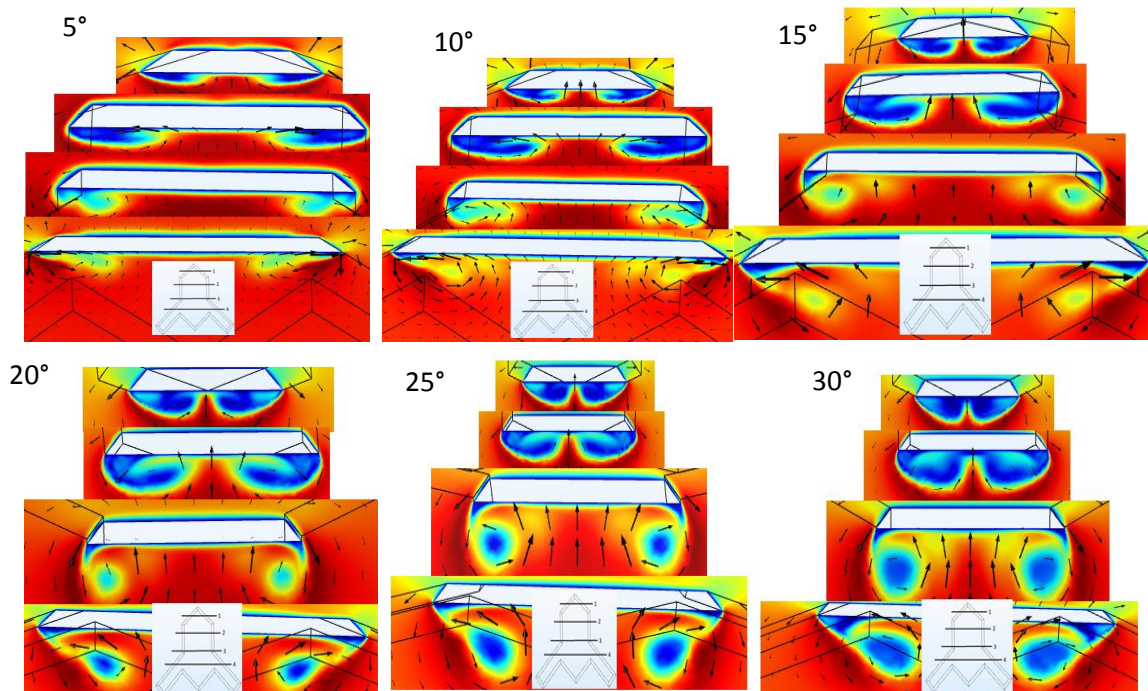


Figure 6:
Comparison of end view pattern of velocity field as a function of angle of attack

Figure:6 provides end view velocity pattern on the section 0.125 , 0.25 and $0.5x/c$ respectively. Eddy flow over the wing surface develops at 5° attack angles and occurs close to the wing

surface and become more prominent up to 20° then vortices on both sides starts to merge into a single one at 25° , and expands over the surface with increasing angle of attack up to 30° . Swirling flow is visible at the angle of 10° and increases intensity up to 30° . As the angle of attack increases, the velocity field shift to the central part, and magnitude increases. Streamline topology indicates that two negative and positive convergent lines are formed in the section near the wing edge and wing center and distance gradually decreases as the angle increase. When the angle of attack reached 30° , flow symmetry was disturbed and a new vortex was formed near the apex and the same situation was observed in numerical calculation. The pattern of dark and light lines shows the positive and negative vorticity contour. There is a pair of spiral counter-rotating vortices that emanates from the leading edge. The extended vorticity lines along the front edge of the wing are associated with the separation of the three-dimensional boundary layer from the wing surface. A similar CFD calculation was conducted for Boeing 1301 UCAV at a variety of angles of attack up to 40° (Cummings et al. 2008) and a streamline velocity field was presented for the upper surface. LEV was developed at the angle attack 10° and the size of circulation increased up 15° and vortex breakdown happened at the halfway of the leading edge. Similarly, the vortex breakdown occurred in approximately the same position as seen in Figure.2 ($\alpha=15^\circ$). At 20° vortex breakdown locations shifted to the apex and the same behavior with the current study, streamline was interrupted and stalled at 30° . Numerical vorticity pattern (Fig. 4) at the angle of 25° proves that another vortex emanating close to the apex which is covering the entire surface and eliminated the LEV at 30° . Aerodynamic characteristics of X45A-wings are rarely found in the literature but Elkhoury et al. (2005) investigated X45-A experimentally at the Reynolds number from 10,000 to 20,000 at the angle of attack 7° and 13° . LEV was developed in both condition and vortex breakdown observed at the halfway and close to leading-edge respectively in dye visualization but in this study, LEV is observed angle of attack up to 25° as seen in Figure. 2-8.

4. CONCLUSION

The effect of angle of attack on the near-surface flow field pattern of X45-A planform was investigated numerically in terms of side and end view streamline topology, vorticity contour. At the lower angle of attack, leading-edge vortices were developed and located very close to the surface of the planform and likely interact with the boundary layer surface. Even though it is very small in size and close to the surface, the leading-edge vortex is visible at the angle of attack 5° and vortices keep their flow configuration up to 25° and stalls at around 30° . Both referenced experiment and numerical method were continued up to 30° since they did not give logical results higher than 30° where dual circulating leading-edge vortex began to unite and turned into a single large vortex in the plan view and end view image. Besides, as seen in the vorticity figures, a third vortex next to the double LEVs begins to form at 25° close to the apex and it covers the entire surface at around 30° .

CONFLICT OF INTEREST

Authors approves that to the best of their knowledge, there is not any conflict of interest or common interest with an institution/organization or a person that may affect the review process of the paper.

AUTHOR CONTRIBUTION

Haci Sogukpinar determined the concept and design process of the research and research management and data analysis and interpretation of results. Serkan Cag did data collection and analysis.

ACKNOWLEDGMENT

Many thanks to Adiyaman University and Middle East Technical University for technical support.

REFERENCES

1. Lambourne, N.C., and Bryer, D.W. (1961). The Bursting of Leading-Edge Vortices – Some observations and Discussion of the Phenomenon. ARC R&M 3282.
2. Sarpkaya T. (1971) Vortex breakdown in swirling conical flows. AIAA J:9(9):1792±9.
3. Faler J.H., Leibovich S. (1978) An experimental map of the internal structure of a vortex breakdown. J Fluid Mech;86(2):313±35.
4. Sahin, B., Tasci, M. O., Karasu, I., & Akilli, H. (2017). Flow structures in end-view plane of slender delta wing. In EPJ Web of Conferences (Vol. 143, p. 02099). EDP Sciences.
5. Canpolat C., Yayla S., Sahin B., Akilli, H (2012). Observation of the Vortical Flow over a Yawed Delta Wing, Journal of Aerospace Engineering, Vol.25, pp. 613-626.
6. Yaniktepe, Bulent, Coşkun Ozalp, And Cetin Canpolat. (2016) Aerodynamics and Flow Characteristics of X-45 Delta Wing Planform. Kahramanmaraş Sutcu Imam University Journal of Engineering Sciences 19.1: 1-10.
7. Swan, Sarah (2006). X-45A Unmanned Combat Vehicle on Display. Aerotech News and Review.
8. Elkhoury, M., Yavuz, M. M. and Rockwell, D., (2005). Near-Surface Topology of a Unmanned Combat Air Vehicles Planform: Reynolds Number Dependence. Journal of Aircraft, Vol. 42, No. 5, pp. 1318-1330.
9. Canpolat C., Yayla, S., Sahin, B., and Akilli, H. (2009). Dye Visualization of the Flow Structure over a Yawed Non-slender Delta Wing, Journal of Aircraft ,Vol. 46, No. 5.
10. Yaniktepe, B., and Rockwell, D. (2004). Flow Structure on a Delta Wing of Low Sweep Angle AIAA Journal, Vol. 42, No. 3.
11. F.R. Menter, (1994) Two-Equation Eddy-Viscosity Turbulence Models for Engineering Applications, AIAA Journal, vol. 32, no. 8.
12. F.R. Menter, M. Kuntz, and R. Langtry, (2003) Ten Years of Industrial Experience with the SST Turbulence Model, Turbulence Heat and Mass Transfer, vol. 4.
13. Sogukpinar, H. (2019) Numerical Investigation of Influence of Diverse Winglet Configuration on Induced Drag. Iranian Journal of Science and Technology, Transactions of Mechanical Engineering 1-13.

14. Sogukpinar, H. (2018). Numerical Calculation of Wind Tip Vortex Formation for Different Wingtip devices. *INCAS Bulletin*, 10(3).
15. Sogukpinar, H. (2019) Low speed Numerical Aerodynamic Analysis of New Designed 3D transport Aircraft. *International Journal of Engineering Technologies*, 4(4), 153-160.
16. COMSOL CFD module user guide. <http://www.comsol.com>. (Access time: February 2022).
17. Cummings, Russell M., Scott A. Morton, and Stefan G. Siegel. (2008) Numerical prediction and wind tunnel experiment for a pitching unmanned combat air vehicle. *Aerospace Science and Technology* 12.5 355-364.